

Quantifying Localized Stresses in the Matrix of a Fiber-Reinforced Composite via Mechanophores

Nazmul Haque, Jared Gohl, Chia-Chih Chang, Hao Chun Chang, and Chelsea S. Davis*

Understanding the stress distribution within fiber-reinforced polymers (FRPs) is critical to extending their operational lifespan. The integration of mechanoresponsive molecular force probes, referred to as mechanophores, presents a potential solution by enabling direct monitoring of stress concentrations. In this study, spiropyran (SP) mechanophores (MPs) are embedded within a polydimethylsiloxane (PDMS) matrix to visualize stress localization during loading within a single fiber-reinforced framework. The SP mechanophore undergoes a transition from a non-fluorescent state to an active state (merocyanine) through isomerization in response to mechanical forces. Using a single fiber mounted axially within the matrix, the fundamental failure modes observed in conventional fiber-reinforced composites are replicated. Samples are strained under uniaxial tensile loading along the fiber direction and the localization of stresses is observed via MP activation. Stresses are concentrated in the matrix near the fiber region that gradually decreases away from the fiber surface. Confocal microscopy is used to visualize mechanophore activation and quantitatively assess fluorescence intensity. Finite element modeling is used to develop a calibration to quantify the stresses based on the observed fluorescence intensity. These outcomes underscore the viability of employing these mechanoresponsive molecules as a potential means to visualize real-time stress distribution, thereby facilitating the design of high-performance composites.

1. Introduction

Composites are widely used in our everyday lives. Various reinforcing materials, ranging from particles to fibers, can be

N. Haque, J. Gohl, C. S. Davis
School of Materials Engineering
Purdue University
West Lafayette, IN 47906, USA
E-mail: ChelseaD@udel.edu
C.-C. Chang, H. C. Chang
Department of Applied Chemistry and Center for Emergent Functional
Matter Science
National Yang Ming Chiao Tung University
1001 Ta Hsueh Road, Hsinchu 30010, Taiwan

The ORCID identification number(s) for the author(s) of this article can be found under https://doi.org/10.1002/macp.202300298

© 2023 The Authors. Macromolecular Chemistry and Physics published by Wiley-VCH GmbH. This is an open access article under the terms of the Creative Commons Attribution-NonCommercial License, which permits use, distribution and reproduction in any medium, provided the original work is properly cited and is not used for commercial purposes.

DOI: 10.1002/macp.202300298

incorporated into a polymer to compose polymer matrix composites (PMCs) tailored to the end-user's requirements. Among PMCs, fiber-reinforced polymers (FRPs) are engineered materials that have been an area of active investigation for decades. The FRPs comprise a polymeric matrix strengthened by the addition of fibers commonly formed of carbon, glass, or polyaramids. FRPs provide an optimal materials system by combining the toughness of the polymer with the stiffness of the reinforcing fibers, which can sustain high loading while maintaining their lightweight nature.[1] Because of this high specific strength, FRPs have been widely applied in many sectors, including the automotive, aerospace, energy, naval, and sports equipment industries. Moreover, the resulting advanced FRPs possess physical and thermomechanical properties unique to the polymer matrix or reinforcing fibers. As a result, the demand for composites is growing quickly, surpassing the industry's capacity to meet this demand.[2] The tremendous demand is caused by the number and variety of composites needed and the extremely high performance standards required.

The overall performance and properties of FRPs hinge on and are affected by stress transfer from the matrix to the fibers across the composite interface. As stress transfer is critical to the performance of composites, it requires special attention during the design and processing steps. In load-bearing FRPs, the reinforcing fibers support most of the load, while the matrix binds the fibers together and facilitates an efficient load transfer between them. However, inefficient stress transfer can potentially lead to the failure of the composites. [3] Failure can initiate and propagate through a combination of factors such as insufficient interfacial adhesion causing fiber/matrix debonding, or even fiber fracture. Moreover, the nonuniform distribution of the loads near the reinforcing fibers during mechanical loading can lead to significant stress localizations and cause sudden catastrophic damage. [4,5] Therefore, it is critical to understand the locations and mechanisms of stress concentrations developed in the matrix near fiber/matrix interfaces within a loaded composite to enable better design and optimize the performance of the FRPs.

The heterogeneous and anisotropic nature of FRPs presents significant challenges to the measurement and analysis of these stress concentrations. Several experimental methods, such as



photoelasticity or birefringence, [6,7] digital image correlation (DIC), [8,9] and X-ray computed tomography (XCT), [10,11] are currently used to assess local stresses or strains within FRPs. Fullfield photoelasticity measurements utilize conformational rearrangement of the polymer chains to modify the birefringence patterns and capture a projection of the stresses through the sample thickness. However, it needs intricate mathematical calculations and assumptions to translate the observed fringes into meaningful relevant stresses.^[12] In digital image correlation, speckle patterns with high-contrast are added to the sample surface, and their mobility is tracked to identify local strains. The measured strains are then used to determine the stress field in the sample. The challenge with DIC is that it presupposes homogeneous strains through the sample's thickness, making it complicated to evaluate internal stress concentrations.^[8] Using the 3D particle tracking technique that extends the traditional DIC methods to volumetric data, tracking particles within a 3D volume becomes possible, providing a comprehensive understanding of complex motion fields.[13,14] In comparison, XCT provides improved spatial stress distribution, as it records sequential images from various angles to construct a 3D image highlighting the changes in internal density distribution and microstructural characteristics. However, it is limited by sample size, phase contrast, and a long acquisition time.[15]

Researchers have recently started employing mechanoresponsive molecules or mechanophores as self-reporting stress sensors in polymeric materials. [16–26] Mechanophores (MPs) are a particular class of stimuli-responsive materials that undergo a chemical change in response to mechanical stimuli. They can be incorporated into the backbone of a polymer chain or crosslinked into a polymer network. [27,28]

Among the wide variety of MPs, spiropyran (SPN) has been studied most significantly in different polymeric systems. The C-O spiro link between the indole and benzopyran sides breaks during the mechanical deformation of SPN-containing materials.[29] The SPN rearranges into the merocyanine form, leading to a change in color and fluorescence. The fluorescence intensity of an SPN-functionalized polymer increases with added mechanical deformation as new populations of mechanophore transition into the fluorescent merocyanine form and are "activated". The activation of the MPs rises along with the applied load (P). Therefore, the strongest MP activation can be detected in the regions of greatest P or stress (σ), allowing the detection of a stress distribution using colorimetric or fluorescence investigations. Utilizing laser scanning confocal fluorescence microscopy to detect this activation signal, we can achieve high 3D spatial resolution of the stresses.[30,31]

Several studies have utilized MPs in different polymeric materials to analyze stresses based on MP activation. [21,32–36] Incorporating MPs with the FRPs lets us get more detailed information on stress accumulation and distribution to investigate composite damage initiation. Several aspects of polymer composite deformation have been previously investigated. MPs have been incorporated into polymer nanofibers reinforced with a bulk polymer matrix. [32] In another study, researchers incorporated spirolactam MP into a ductile epoxy polymeric matrix. The fluorescence lifetime images of the MPs revealed matrix-yielding and extensive localized stress approximately two fiber diameters away from the fracture site during fiber fragmentation. [37] Additionally,

MPs have been added to the fiber surface to understand interfacial debonding in the FRPs.^[38,39] Placing interfacial MPs at the interface between the reinforcing fiber and the matrix allows the detection of micron-length scale separations, including fiber fracture and debonding at the interface.^[26] Applying a uniaxial tensile loading to the composite caused deformation at the interface, leading to fluorescent activation of the mechanophore.

work has previously utilized MPs for stress sensing.[21,27,28,39,40] One major issue with the commercialization of MPs is quantifying MP activation and relating it to stress. In an effort to quantify the MP activation, Celestine et al. carried out a fracture experiment on MP-functionalized rubber toughened PMMA. They established a power law relationship between stress (σ) and intensity (I), utilizing strain fields obtained via DIC.[41] Recently, Clough and coworkers proposed a protocol utilizing supramolecular mechanophores and confocal microscopy to characterize strain distribution via mechanophore activation.^[42] In a different study, Chen et al. mapped the stress field in front of a propagating crack using finite element analysis (FEA). They discussed that the strain field measurements and constitutive models might not be accurate when there are abrupt gradients and the material acts very nonlinearly at high stresses. [43] In our previous studies, we demonstrated a systematic methodology to calibrate the stresses in polymer composites by correlating calculated stresses from FEA with experimentally observed MP fluorescent activation intensities of the same material system.^[21,40] The calibration was accomplished by embedding stiff spherical silica particles into an SPN-functionalized silicone elastomeric matrix. When loaded, the rigid inclusion caused stress localizations in the matrix that exceeded the fracture strength of the matrix. The observed fluorescent intensity images were correlated with the maximum principal stresses from FEA.[40] The Ogden hyperelastic model was used to represent the polymer matrix in FEA. This calibration, correlating maximum principal stress (σ_{m}) to intensity (I), enables direct quantification of the stresses in the system. One of the objectives of the current work is to adapt our previously established calibration method to analyze a different composite geometry and reinforcing material, all while maintaining the same optical imaging conditions employed in previous research. By doing so, we seek to streamline the process of assessing stress within more intricate composite systems. Instead of conducting multiple calibration experiments for each new composite, the aim was to use a single calibration experiment as a reference point. Thus, we will demonstrate the possibilities of running a single "glass sphere in a matrix" calibration experiment to quantify stress in experiments with more complex shapes, mixed mode loading conditions, and reinforcement geometries. This would allow efficient quantification of stress in a range of complex composite materials, demonstrating the universality of this approach for future studies in composite materials research.

In this work, we delved into understanding the magnitude of stress in the matrix of an FRP and sought to apply the σ to I calibration approach for quantitative evaluation of the stresses in the matrix from previous studies to a composite with a different reinforcing phase and sample geometry. We have fabricated a fiber-reinforced polymer composite by embedding a single fiber in an SPN-functionalized polydimethylsiloxane (PDMS) elastomeric matrix. **Figure 1** shows this experimental approach



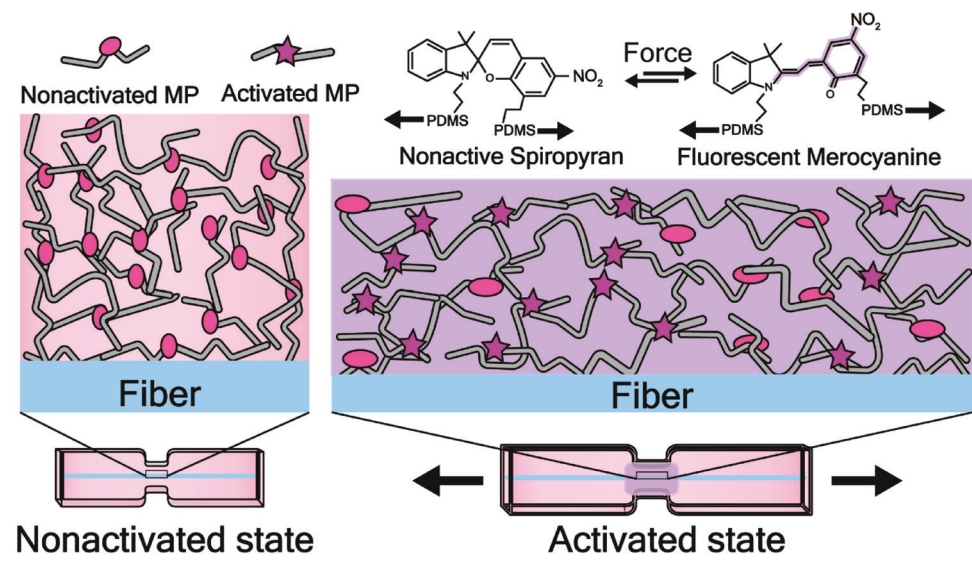


Figure 1. Schematic representation of a single fiber reinforced polymer (PDMS) composite where mechanophores were crosslinked with the PDMS matrix. When an external load is applied to the composite, it proportionally translates into MPs through the polymer chains. A representative MPs spiropyran (SPN) molecular structure has also been represented in its nonactivated state and force-induced activated fluorescent merocyanine state.

and illustrates the functionalization and stress-induced activation mechanism of the MP-functionalized polymer matrix in a single fiber tensile specimen. We employed in situ micromechanical testing coupled with confocal microscopy, where we observed MP activation in the single fiber composites subjected to uniaxial tensile load.

We have measured the magnitude of localized stresses in the matrix of a fiber-reinforced polymer composite via MP activation. Using the previously developed calibration method for mechanophore activation, we then calibrated the experimentally obtained fluorescence images to produce a quantitative stress map. The systematic stress quantification method described here offers the ability to observe and quantify stress localizations in complex composite systems like FRPs during loading.

2. Experimental Section

An elastomeric matrix of PDMS was functionalized with MPs. Single fiber composite tensile specimens were then prepared by embedding a polyaramid fiber along the long axis of each specimen within this functionalized polymer matrix. An in situ testing approach was adopted, which allowed mechanical testing to be coupled with fluorescence microscopy. Each sample was loaded in tension under precise displacement control while monitoring the resulting tensile response. During this process, confocal microscopy was employed to observe and quantify the MP fluorescent activation. Finally, finite element simulations were employed to compare the calculated stress in the matrix with the observed MP activation intensity to calibrate the stress response of the MP-PDMS.

2.1. Sample Preparation and Fiber Laying Protocol

PDMS elastomer (Sylgard 184 Silicone, Dow) was used as the matrix of FRP, where the base and curing agent were mixed in a 10 to

1 ratio by mass. Nitro-spiropyran (SPN, 0.6 wt%) mechanophore was added to the elastomer to functionalize the matrix. The SPN was synthesized and incorporated into the PDMS following previously reported procedures. $^{[21]}$ At this concentration, there were approximately 6.6 \times 10 6 SPN molecules per μm^3 , with a calculated average spacing between each molecule of 6.6 nm. A two-step mixing procedure was established to prepare the matrix. Briefly, the mechanophore was dissolved in xylenes (99%, ACS Reagent, Acros Organics) at a concentration of 0.05 g mL $^{-1}$ to improve solubility before being added to the PDMS elastomer base. Next, this mixture was vortex mixed (LP Vortex Mixer, Thermo Scientific) for 60 s to establish homogeneity, then the crosslinker was added and vortex mixed for an additional 60 s. Finally, the uncured PDMS mixture was placed under a vacuum for 600 s to eliminate air bubbles.

Commercially available polyaramid monofilament (Supplemax, Beadalon) with a 250 μm diameter was used as the reinforcing material for all experiments. A systematic methodology for preparing single-fiber reinforced polymer samples while ensuring the fiber is positioned at the thickness center of the sample was developed.

This process involved the fabrication of a 1 mm thick rectangular mold from glass microscope slides. Two 5 mm wide by 0.5 mm thick metal strips were used on opposing ends of the mold to ensure proper fiber placement. These metal strips acted as anchors for the fiber, enabling fiber alignment and location of each fiber in the cross-sectional centroid of each tensile specimen. A single fiber with a diameter of 250 μm was then adhered to the metal strips using invisible office adhesive tape. The fiber was pre-strained to approximately 5% before attachment to prevent buckling during matrix casting and curing. This precaution ensured the fiber was not damaged and was correctly positioned during fabrication. The step-bystep sample preparation stages are shown in the schematic of Figure 2a.

15213935, 0, Downloaded from https://onlinelibrary.wiley.com/doi/10.1002/macp.202300298, Wiley Online Library on [08/11/2023]. See the Terms and Conditions (https://onlinelibrary.wiley.com/terms-and-conditions) on Wiley Online Library for rules of use; OA articles are governed by the applicable Creative Commons Licensea

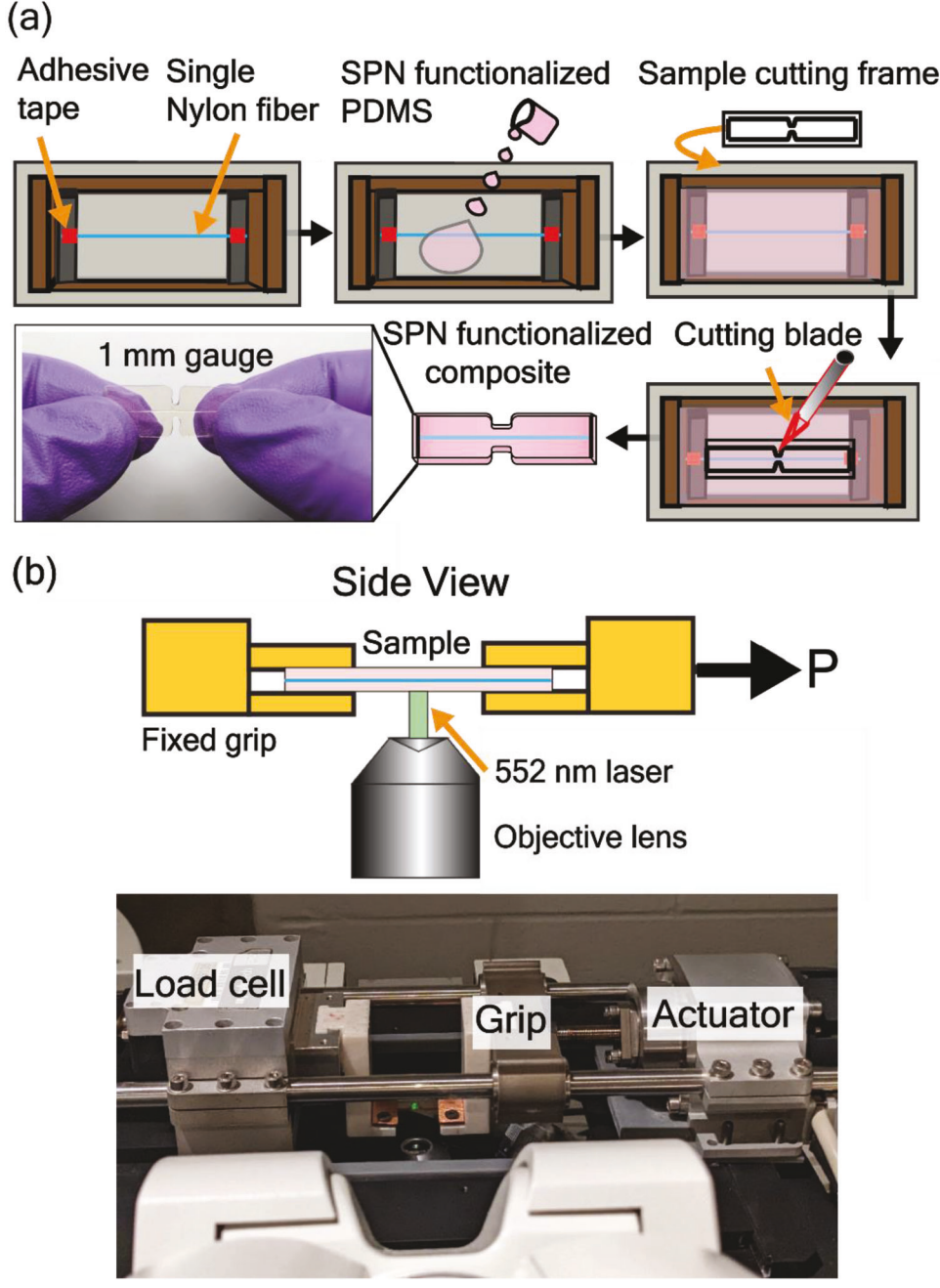


Figure 2. a) Schematic representation of the sample preparation stages where the SPN functionalized PDMS was poured into the mold containing a single fiber glued on the two edges. The single fiber reinforced composite sample was cut out of the mold having a specific 1 mm gauge length. b) In situ testing set up with a tensile frame on top of a confocal microscope allowing continuous monitoring of MP activation during loading.

Next, the SPN-MP functionalized silicone elastomer was poured into the master mold to prepare the composite. Then, it was placed on a flat surface, allowing enough time for the polymer to fully fill the corners of the mold, ensuring equal distribution and complete fiber impregnation. After filling the mold, the sample was placed in a vacuum oven at a pressure of 380mmHg. The samples were cured for 24 h at 70 °C. The vacuum environment aided in the removal of any trapped air bubbles. Finally,

a dogbone-shaped cutting mold with a 1 mm gauge length was employed. The composite samples were hand-cut using a scalpel.

2.2. In Situ Tensile Testing and Confocal Microscopy

An in situ tensile testing setup was utilized comprised of a micromechanical load frame and a confocal laser scanning

microscope. The activation of the MP was observed while loading our single-fiber composites, enabling us to analyze the stress build-up via MP activation intensity. The mechanical testing setup is shown in Figure 2b highlighting the loading direction. The composite samples with 1 mm gage length were securely attached to the load frame (μ TS, Psylotech) using custom 3D-printed grips to maintain a proper working distance between the sample mid-plane and the microscope objective throughout the studies. The load frame was then carefully attached to a custom microscope stage insert, allowing for facile transfer of the load frame to its position above the inverted microscope objective.

Uniaxial tensile loading was applied to the samples along the fiber direction at a strain rate of $0.001~\rm s^{-1}$ (a global displacement rate of $10~\mu m \cdot s^{-1}$) until failure. A laser scanning confocal microscope (SP8, Leica Microsystems) was used to monitor and visualize MP fluorescent activation during loading. An air objective ($20\times$, NA = 0.40) with a long working distance (WD = $6.9~\rm mm$) was used for all tests. Sample excitation was achieved with a solid-state laser (λ = $552~\rm nm$) with a 1 mW laser output power. This laser emission was selected as it corresponded to the absorbance peak of SPN in PDMS observed with a solid-state fluorimeter. A photomultiplier tube (PMT) was used to record the emission of the activated MP. With a gain of 600 mV, a wide emission band was selected to measure emission wavelengths from 600 to 725 nm.

Images were taken at the mid-plane of the sample, enabling a detailed view of the stress localization and debonding events within the loaded sample. Images measuring 581 by 581 μm had a resolution of 1.14 by 1.14 μm . For all experiments, the pinhole was set to 1 Airy Unit, yielding a depth of field for a single confocal slice of 7.23 μm . Images were acquired every 1.5 s. The focus was adjusted manually with each sequential mechanical displacement step to ensure that the focal plane of the image remained directly at the mid-plane of the fiber. Since the sample was nearly incompressible, the fiber mid-plane moved only slightly and systematically with each sequential strain step. Moreover, the fluorescence intensity was normalized to analyze and compare mechanophore activation across the samples.

In addition to confocal microscopy, the bright-field and epifluorescence microscopic images were also looked at using a similar microscope (DMi8, Leica Microsystems) with 5× magnification to have a broader aspect on stress initiation and distribution. Both of these images were captured using an exposure time of 450 ms. A Y3 filter cube set (Ex: 532–558 nm and Em: 570–640 nm) was used for epifluorescence imaging to capture the MP activation.

3. Results and Discussion

We tested single-fiber FRP composites with mechanophores in the matrix and a single nylon fiber as reinforcement in order to assess the development of stresses in the matrix of a loaded composite system. While putting the specimens under uniaxial tension, the resulting fluorescence activation intensity was observed in situ. To quantitatively assess the stresses within the system, we used a previously developed calibration approach. [40] This calibration method allows quantitative measurements of stresses developed in an MP-containing sample assuming fixed imaging conditions and mechanophore content between samples. MP activation/stress calibration was achieved by determining a correlation

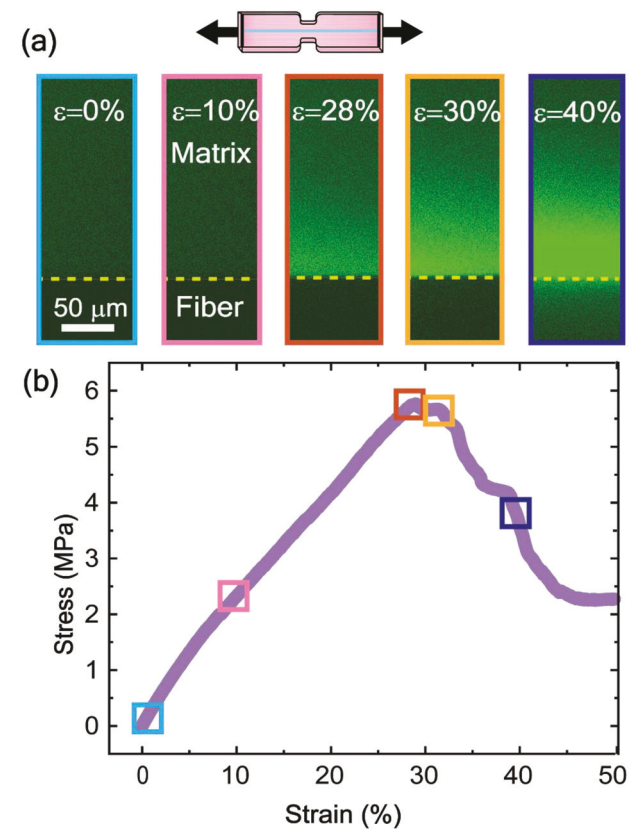


Figure 3. The fluorescence intensity of the MP in the matrix near the fiber increased as a function of applied tensile strain. a) Sequential fluorescence images show how the MP activates as the stress localizes in the matrix near the fiber surface during loading. b) Representative stress-strain plot highlighting different stages of MP activation indicated with open squares. Colors correspond to the images in (a).

between the experimental fluorescence micrographs at varying loadings and the calculated stress distributions predicted from the FEA model at corresponding strains. Mapping this correlation between observed MP intensity and calculated stresses onto images of deformed MP samples results in a final quantitative stress map based on MP activation intensities which indicates the concentration and distribution of stress in the FRPs.

3.1. Analyzing the Tensile Test Results

Several material and scientific processes occurred when the single fiber-reinforced composites were subjected to a uniaxial tensile load with the fiber oriented in the direction of loading. In the early stages of the loading, the polymer matrix surrounding the fiber began to deform elastically. This phenomenon is shown in **Figure 3**a, where various stages of loading are highlighted. As the specimen was stretched further, the polymer chains in the matrix started to align in the direction of the applied load. The way polymer chains rearrange themselves here can be referred to as strain-induced orientation. Interfacial shear stress developed at the interface between the matrix and fiber.

The fiber carries the majority of the applied load since it has a significantly higher modulus than the matrix material.



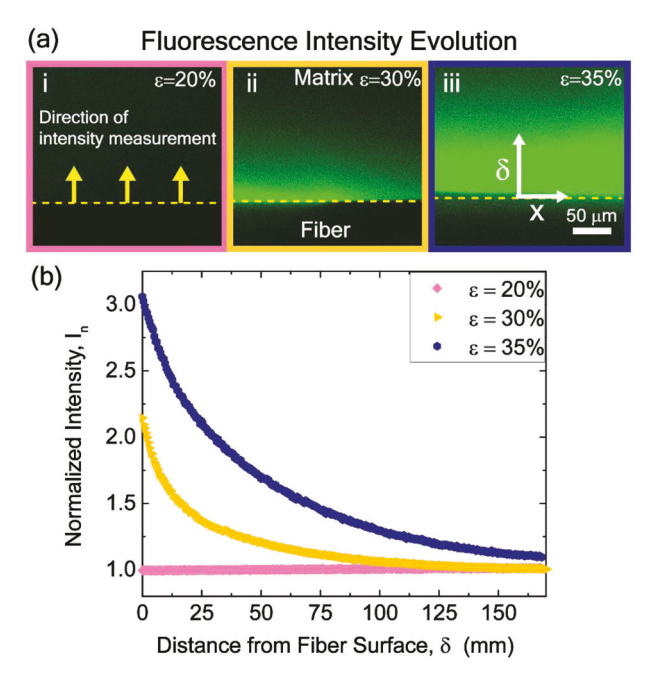


Figure 4. Analyzing activation intensities at different strains; a) Fluorescent intensity images at different strains indicating the direction of intensity measurement. b) The plot shows the overall MP activation intensity decreases outward from the fiber surface into the matrix.

However, the mismatch in mechanical properties caused a stress concentration at the interface between the fiber and matrix. This stress concentration eventually resulted in interfacial debonding at higher loadings, leading to partial or complete matrix separation from the fiber. We observed a monotonic increase in the force up to a strain of 30%, at which point the load decreased in a sequence of small rapid failures as the strain increased further. These drops in stress were directly correlated with the microscope observations of interfacial debond initiation and eventual fracture of the matrix.

While MP intensity was strongest near the fiber surface, the stress in the surrounding matrix as a function of distance from the fiber gradually decreased as shown in Figure 4. The reduction in stress in the matrix far from the fiber surface can be attributed to the matrix material's lower modulus than the fiber.

Another observation of this study was how debonding propagated from the stationary side of the sample across to the actuating side of the sample. The portion of the sample near the fixed end experienced more stress due to the applied load intensity. Figure 5 compares the brightfield, epifluorescence, and fluorescence images that highlight the debonding initiation and propagation capturing fluorescent activation of MPs. The load gradually passed through the composite material as it was applied to the moving end (the area where the load was initially applied). The stress was redistributed along the length of the composite as the strain increased. As the load was transmitted along the fiber and matrix, the moving end experienced a more uniform distribution of stresses. The debonding initiation and propagation occurred very quickly and happened within a range of 5% increase in strain. On the other hand, the stationary end experienced a higher stress concentration because of the lack of movement and

Macromol. Chem. Phys. 2023, 2300298

the resulting stress redistribution. As a load-bearing component, the continuous nylon fiber in the composite transmitted the applied load from the moving end to the fixed end. However, there was a delay in the transmission of the load to the fixed end.

The complicated stress evolution observed here might be explained differently. Beginning with the fiber debonding from the matrix close to the stationary pole, the Poisson effects cause the matrix to contract radially. As the matrix contracts, the fiber is compressed and encounters higher friction as it is pulled through the cored region where the thermoset matrix is cured around the undeformed fiber in a relaxed (0 strain) state. The increased friction leads to increased shear stresses close to the fiber/matrix interface, reported by the mechanophores as increased fluorescence intensity. An analogy of this interfacial separation and increased shear stress mechanism can be drawn from the research conducted by Fourton et al. in an inverse system of an extensional polymer confined between two rigid plates.[44] Their research sought to understand the transition between stable delamination cases and interlayer "rupture" behavior. The results showed that thinner interlayers could resist greater stresses than thicker ones, demonstrating a rivalry between cohesive breakage and adhesive debonding inside the interlayer that is connected to the durability of the polymer material. Their study is another example that demonstrates a deformation mechanism responsible for stresses propagating from a moving grip toward a stationary

3.2. Evaluating MP Activation Intensities

The MP activation intensities provided information on the stress state within the matrix of the loaded composite sample. In the case of our fiber-reinforced polymer composite subjected to uniaxial tensile loading, stress propagated throughout the material as the polymer matrix deformed in response to the applied load. A fluorescence response resulted from the strain-induced deformation and subsequent molecular structural change experienced by the mechanophores due to their crosslinking with the polymer matrix. As the MPs were uniformly distributed throughout the PDMS network, they are expected to respond in an affine manner to any external loading. More MPs in the system activated as the deformation increased, increasing the observed intensity of the chromatic or fluorescence response.

We observed the highest localized stress near the fiber and matrix interface. This localization of stress occurred because the matrix bound to the fiber surface was unable to deform elastically with the bulk of the matrix, giving rise to larger stresses developing in the matrix. Figure 4 highlights different stages of the MP activation and how the activation intensities changed over in the matrix as a function of distance from the fiber surface. Intensity values were measured along a 3 mm wide line over a length of 20 mm using image analysis software (Image], National Institutes of Health). The onset of the MP activation was observed between 20% and 25% strain, where a high-stress localization at the fixed end of the specimen was observed to activate first. As we applied more load, at higher strains around 30%, we observed a significantly higher intensity. With the application of 5% more strain, we noticed a jump in activation about 200% from initially noted intensities at 25% strain. We applied a normalization

5213935, 0, Downloaded from https://onlinelibrary.wiley.com/doi/10.1002/macp.202300298, Wiley Online Library on [08/11/2023]. See the Terms and Conditions (https://onlinelibrary.wiley.com/terms-and-conditions) on Wiley Online Library for rules of use; OA articles are governed by the applicable Creative Commons Licensea and Conditions (https://onlinelibrary.wiley.com/terms-and-conditions) on Wiley Online Library for rules of use; OA articles are governed by the applicable Creative Commons Licensea and Conditions (https://onlinelibrary.wiley.com/terms-and-conditions) on Wiley Online Library for rules of use; OA articles are governed by the applicable Creative Commons Licensea and Conditions (https://onlinelibrary.wiley.com/terms-and-conditions) on Wiley Online Library for rules of use; OA articles are governed by the applicable Creative Commons Licensea and Conditions (https://onlinelibrary.wiley.com/terms-and-conditions) on Wiley Online Library for rules of use; OA articles are governed by the applicable Creative Commons Licensea and Conditions (https://onlinelibrary.wiley.com/terms-and-conditions) on Wiley Online Library for rules of use; OA articles are governed by the applicable Creative Commons Licensea and Conditions (https://onlinelibrary.wiley.com/terms-and-conditions) on Wiley Online Library for rules of use; OA articles are governed by the applicable Creative Commons and the conditions of the conditions

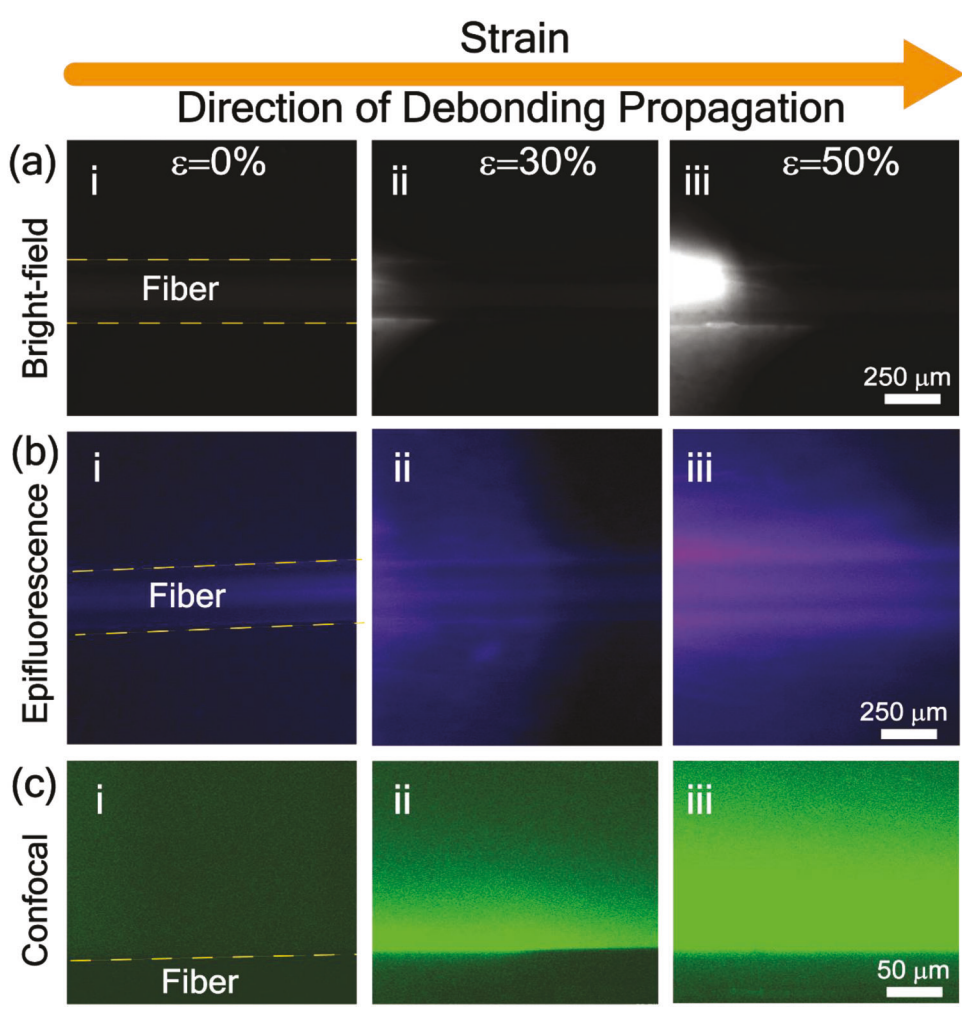


Figure 5. Evolution of stress observed around the fixed end of the tensile specimen during loading started at the fiber surface and extended into the matrix, migrating in the strain direction. The interfacial debonding initiation and propagation between the matrix and fiber are shown in a) brightfield, b) epifluorescence, and c) confocal imaging modes with increasing strains. Brightfield and epifluorescence images highlight the direction of debonding propagation and activation of MPs in the matrix around the fiber surface and were acquired during the same experiment. The confocal images were acquired at a higher magnification and showed the concentration of stress through changes in MP activation intensity.

procedure for better comparison of the intensities by dividing the activation intensity with the background intensity at 20% (no detectable MP activation). The normalized intensities (I_n) at strain 30% and 35% at a distance δ into the matrix from the fiber surface followed the Stirling function of nonlinear exponential growth that could be represented by Equation (1).[45]

$$I_n = a + b \left(\frac{e^{k\delta} - 1}{k} \right) \tag{1}$$

The parameters b and k are the coefficients where $b = -0.0402 \pm 3.938E^{-4}$ to $0.0338 \pm 6.774E^{-4}$, k $-0.0218 \pm 1.911E^{-4}$ to $0.0359 \pm 5.295E^{-4}$, and offset a = 2.9163 ± 0.006 to 1.9700 ± 0.007 .

The stress progressively decreased away from the fiber surface and deeper into the matrix. As the load was spatially transferred away from the fiber, this drop in activation intensity represented the matrix's relaxation and stress redistribution.

Additionally, the observation of strong MP activation adjacent to the fixed end, where debonding was initiated, revealed insight into how interfacial failure occurred during loading in the composite. Figure 6 compares the activation intensities between the two ends of the sample. We noted about 33% higher activation intensity at the fixed compared to the loading pole at a lateral spacing of just 200 µm. This elevated MP activation intensity at the fixed end led to the localization of stress and the initiation of debonding.

3.3. Quantifying I to σ

Utilizing a previous calibration method, [21,40] which established a link between the intensity of experimental MP activation and the stress calculated by FEA of the similar material system, it was possible to measure stress based on MP activation. A comparison of the intensities of two systems — a single glass

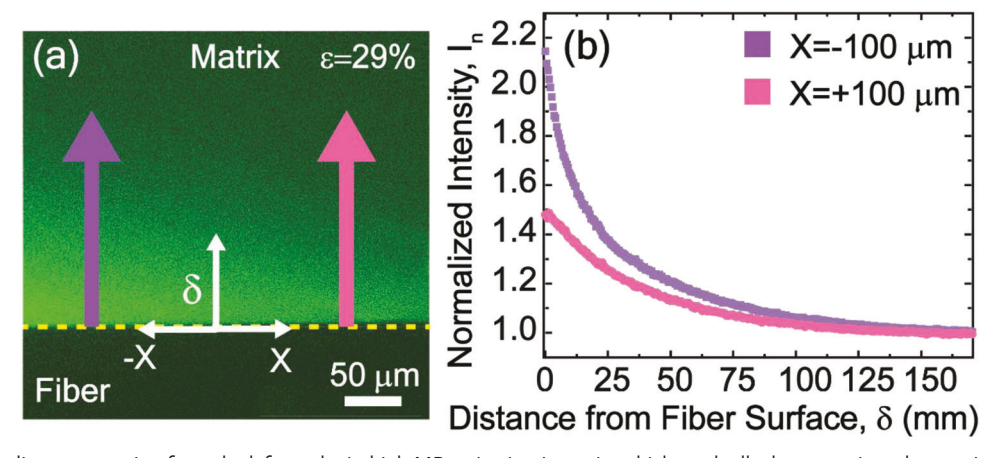


Figure 6. a) Debonding propagating from the left results in high MP activation intensity which gradually decreases into the matrix away from the fiber surface. b) On the left, at $X = -100 \,\mu\text{m}$ the activation intensity is about 33% higher than the right side at $X = 100 \,\mu\text{m}$ which is far from the debonding propagation tip. Note that δ is taken at the horizontal center of the image and used for positioning purposes only for this figure.

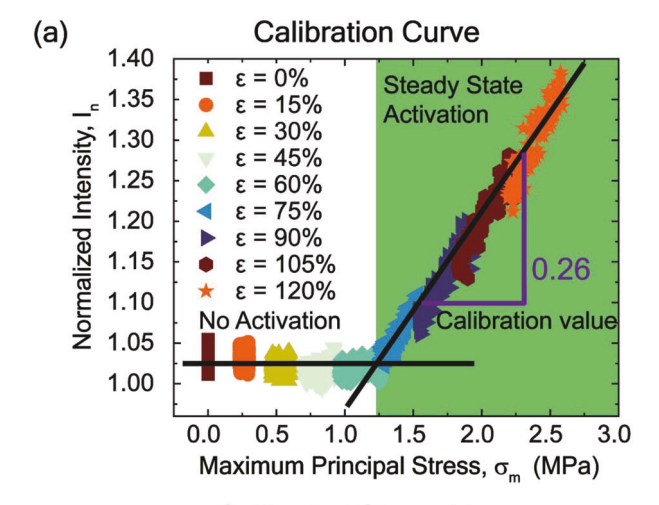
particle-reinforced composite and a single nylon fiber-reinforced composite—each with a matrix composed of 0.6 wt% SPN functionalized PDMS was carried out to employ this calibration. Identical imaging settings were applied to both cases. An equivalent activation response was recorded prior to failure in both systems, illustrating that the MP activation threshold had been reached. The results suggested that the previously established calibration could be used to directly and quantitatively assess the localized stresses in FRPs. The Supporting Information contains more calibration details and results from these experiments. To develop the calibration, we compared the experimentally obtained MP fluorescent activation intensity values with the maximum principal stresses from FEA at different strain levels. As shown in Figure 7a, the calibration shows two regimes: one with no change in I to σ and another linear steady-state regime. The slope of the steady-state regime (0.26 \pm 0.002 MPa⁻¹) was taken as the calibration value for our FRP system.

The derived calibration value was superimposed onto the intensity images experimentally to generate a stress map. The stress values range from 1.2 to 2.5 MPa as highlighted in the calibrated stress map shown in the Figure 7b. This procedure made it possible to translate qualitative observations of fluorescence intensity into quantitative stress values, resulting in a visual representation of the stress distribution throughout the matrix.

Understanding the stress localization and mechanical response of the matrix in FRPs required a thorough understanding of the intensity of stress calibration. This approach directly evaluates stress utilizing experimental data by establishing a link between fluorescence intensity measurements and the related stress levels. Furthermore, this calibration established the accuracy and dependability of the fluorescence-based stress sensing approach by bridging the gap between experimental data and numerical simulations.

4. Conclusion

By incorporating mechanophores in an FRP, we visualized and quantified stress at the micron length scale detailing the mag-



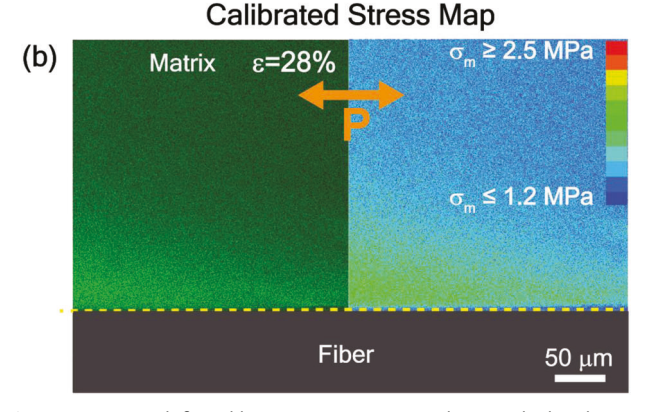


Figure 7. Approach for calibrating MP intensity with FEA calculated stress to map stresses in experimentally obtained images. a) Calibration was developed by correlation of experimental intensities with FEA stresses. b) Calibrated stress map (right) obtained by applying the calibration value to the experimental fluorescent image (left) showing MP activation and localized stresses at 28% strain, before debonding initiated. The orange double-headed arrow indicates the applied tensile loading direction.

_ Chemistry and Physics www.mcp-journal.de

nitude of stress in the matrix. This information is essential for optimizing composite materials selection, locating areas in a design where stress localizations can occur, and foretelling possible failure modes. Using mechanophores and in situ testing, we directly observed how stress, deformation, and MP fluorescence response in the fiber-reinforced polymer composites occurs. We proposed a methodical procedure to prepare a single nylon fiber-reinforced composite system functionalizing the matrix with MPs. We observed a strong MP activation near the fiber surface caused by high localized stress during the in situ tensile testing, which subsequently decreased as it progressed away from the fiber and deeper into the matrix Additionally, the fixed end of the tensile specimen experienced significant localized stresses, initiating debonding while the actuating end exhibited measurably less stress during loading. This resulted in high MP activation intensity near the fixed end. Moreover, we improved our understanding of the mechanical behavior of FRPs by establishing a direct relationship between MP activation intensity and stress distribution by correlating the fluorescence intensity with the maximum principal stress values obtained from FEA. This intensity-to-stress calibration gives information on the distribution of stress and the efficiency of load transfer in the matrix. In conclusion, this study translated MP fluorescence activation intensity into a visual means of quantitative stress measurement in complex material systems like FRPs. Researchers can better understand the mechanical performance of engineered materials by precisely quantifying stress following the process shown here, which will help with composite system design and optimization.

In the future, we will focus on higher-rate deformation mechanisms by incorporating advanced imaging methods using high-speed cameras and full-field fluorescence techniques. Additionally, we see potential in employing spinning disk confocal microscopy, which is well-suited for our research due to its ability to operate effectively with lower excitation power and quicker data acquisition capabilities. These techniques will enhance our ability to capture detailed data, different deformation modes, and insights for our system at higher strain rates.

Supporting Information

Supporting Information is available from the Wiley Online Library or from the author.

Acknowledgements

N.H., J.G., and C.D. acknowledge support from the NSF-CMMI CAREER (Grant #2045908). H.-C.C. and C.-C.C. acknowledge support from the Young Scholar Fellowship Program by the National Science and Technology (Grant 111-2636-E-A49-015 and 111-2634-F-A49-007) and the Center for Emergent Functional Matter Science of National Yang Ming Chiao Tung University from The Featured Areas Research Center Program within the framework of the Higher Education Sprout Project by the Ministry of Education (MOE) in Taiwan.

Conflict of Interest

The authors declare no conflict of interest.

Data Availability Statement

The data that support the findings of this study are available from the corresponding author upon reasonable request.

Keywords

fiber-reinforced polymer composites, fracture mechanics, mechanophores, polydimethylsiloxane, stress localization

Received: August 15, 2023 Revised: September 23, 2023 Published online:

- [1] F. Ahmad, H. S. Choi, M. K. Park, Macromol. Mater. Eng. 2015, 300, 10.
- [2] D. Rajak, D. Pagar, P. Menezes, E. Linul, Polymers 2019, 11, 1667.
- [3] N. K. Parambil, S. Gururaja, Mech. Mater. 2017, 111, 21.
- [4] J. M. Hedgepeth, P. Van Dyke, J. Compos. Mater. 1967, 1, 294.
- [5] G. P. Carman, R. C. Averill, K. L. Reifsnider, J. N. Reddy, J. Compos. Mater. 1993, 27, 589.
- [6] L. D. Suits, T. C. Sheahan, J. Dijkstra, W. Broere, Geotech. Test. J. 2010, 33, 469
- [7] A. S. Voloshin, C. P. Burger, Exp. Mech. 1983, 23, 304.
- [8] R. Janeliukstis, X. Chen, Compos. Struct. 2021, 271, 114143.
- [9] M. Tekieli, S. De Santis, G. De Felice, A. Kwiecien, F. Roscini, Compos. Struct. 2017, 160, 670.
- [10] J. Vogtmann, A. Klingler, T. Rief, M. Gurka, J. Compos. Sci. 2021, 2021, 121.
- [11] K. Martyniuk, B. F. Sørensen, P. Modregger, E. M. Lauridsen, Composites, Part A 2013, 55, 63.
- [12] M. M. Shokrieh, A. R. Ghanei Mohammadi, in Residual Stresses in Composite Materials (Ed: Mahmood M. Shokrieh), Woodhead Publishing, Oxford 2021.
- [13] M. Gates, J. Lambros, M. T. Heath, Exp. Mech. 2011, 51, 491.
- [14] E. Bar-Kochba, J. Toyjanova, E. Andrews, K.-S. Kim, C. Franck, Exp. Mech. 2015, 55, 261.
- [15] Y. Gao, W. Hu, S. Xin, L. Sun, J. Compos. Mater. 2022, 56, 133.
- [16] D. A. Davis, A. Hamilton, J. Yang, L. D. Cremar, D. Van Gough, S. L. Potisek, M. T. Ong, P. V. Braun, T. J. Martínez, S. R. White, J. S. Moore, N. R. Sottos, *Nature* 2009, 459, 68.
- [17] A.-D. N. Celestine, B. A. Beiermann, P. A. May, J. S. Moore, N. R. Sottos, S. R. White, *Polymer* 2014, 55, 4164.
- [18] Y. Zheng, J. Jiang, M. Jin, D. Miura, F. X. Lu, K. Kubota, T. Nakajima, S. Maeda, H. Ito, J. P. Gong, J. Am. Chem. Soc. 2023, 145, 7376.
- [19] T. A. Kim, C. Lamuta, H. Kim, C. Leal, N. R. Sottos, Adv. Sci. 2020, 7, 1903464.
- [20] Y. Chen, C. J. Yeh, Q. Guo, Y. Qi, R. Long, C. Creton, Chem. Sci. 2021, 12, 1693.
- [21] M. L. Rencheck, B. T. Mackey, Y.-Y. Hu, C.-C. Chang, M. D. Sangid, C. S. Davis, Adv. Eng. Mater. 2021, 24, 2101080.
- [22] S. Yoon, J. H. Choi, B. J. Sung, J. Bang, T. A. Kim, NPG Asia Mater. 2022, 14, 61.
- [23] M. Stratigaki, R. Göstl, ChemPlusChem 2020, 85, 1095.
- [24] M. E. McFadden, M. J. Robb, J. Am. Chem. Soc. 2019, 141, 11388.
- [25] M. A. Ghanem, A. Basu, R. Behrou, N. Boechler, A. J. Boydston, S. L. Craig, Y. Lin, B. E. Lynde, A. Nelson, H. Shen, D. W. Storti, Nat. Rev. Mater. 2020, 61, 84.
- [26] K. Makyla, C. Müller, S. Lörcher, T. Winkler, M. G. Nussbaumer, M. Eder, N. Bruns, Adv. Mater. 2013, 25, 2701.





- [27] C. S. Davis, M. L. Rencheck, J. W. Woodcock, R. Beams, M. Wang, S. Stranick, A. M. Forster, J. W. Gilman, ACS Appl. Mater. Interfaces 2021, 13, 55498.
- [28] N. Deneke, M. L. Rencheck, C. S. Davis, Soft Matter 2020, 16, 6230.
- [29] G. R. Gossweiler, G. B. Hewage, G. Soriano, Q. Wang, G. W. Welshofer, X. Zhao, S. L. Craig, ACS Macro Lett. 2014, 3, 216.
- [30] Y. Chen, G. Mellot, D. Van Luijk, C. Creton, R. P. Sijbesma, Chem. Soc. Rev. 2021, 50, 4100.
- [31] B. A. Beiermann, D. A. Davis, S. L. B. Kramer, J. S. Moore, N. R. Sottos, S. R. White, J. Mater. Chem. 2011, 21, 8443.
- [32] M. Raisch, D. Genovese, N. Zaccheroni, S. B. Schmidt, M. L. Focarete, M. Sommer, C. Gualandi, Adv. Mater. 2018, 30, 1802813.
- [33] X. P. Morelle, G. E. Sanoja, S. Castagnet, C. Creton, Soft Matter 2021, 17, 4266.
- [34] C. M. Degen, P. A. May, J. S. Moore, S. R. White, N. R. Sottos, *Macro-molecules* 2013, 46, 8917.
- [35] C. K. Lee, D. A. Davis, S. R. White, J. S. Moore, N. R. Sottos, P. V. Braun, J. Am. Chem. Soc. 2010, 132, 16107.

- [36] J. R. Hemmer, P. D. Smith, M. Van Horn, S. Alnemrat, B. P. Mason, J. R. De Alaniz, S. Osswald, J. P. Hooper, J. Polym. Sci., Part B: Polym. Phys. 2014, 52, 1347.
- [37] J. W. Woodcock, R. J. Sheridan, R. Beams, S. J. Stranick, W. F. Mitchell, L. C. Brinson, V. Gudapati, D. Hartman, A. Vaidya, J. W. Gilman, G. A. Holmes, Compos. Sci. Technol. 2020, 192, 108074.
- [38] M. E. Grady, C. M. Birrenkott, P. A. May, S. R. White, J. S. Moore, N. R. Sottos, *Langmuir* 2020, 36, 5847.
- [39] J. W. Woodcock, R. Beams, C. S. Davis, N. Chen, S. J. Stranick, D. U. Shah, F. Vollrath, J. W. Gilman, Adv. Mater. Interfaces. 2017, 4, 1601018.
- [40] J. A. Gohl, T. J. Wiley, H.-C. Chang, C.-C. Chang, C. S. Davis, Front. Soft Matter 2023, 3, 1125163.
- [41] A.-D. N. Celestine, N. R. Sottos, S. R. White, Strain 2019, 55, 12310.
- [42] H. Traeger, D. Kiebala, C. Calvino, Y. Sagara, S. Schrettl, C. Weder, J. M. Clough, *Mater. Horiz.* 2023, 10, 3467.
- [43] Y. Chen, C. J. Yeh, Y. Qi, R. Long, C. Creton, Sci. Adv. 2020, 6, aaz5093.
- [44] P. Fourton, K. Piroird, M. Ciccotti, E. Barthel, Glass Struct. Eng. 2020, 5. 397.
- [45] W. D. Stirling, J. R. Stat. Soc., Ser. C 1985, 34, 183.